Norris et al., http://www.jcb.org/cgi/content/full/jcb.201407086/DC1

A

Schematic	Linker	Type	Notes	Reference
	IQ/IA	Antiparallel heterotrimeric coiled-coil (AAB-type)	Worked well in motility and Co-IP screen (Fig. 2, S1)	Kiyokawa et al., 2004
	GCN4 Trimer	Antiparallel homotrimeric coiled-coil; mutant version (N16A) of leucine zipper of yeast transcriptional activator GCN4 (AAA-type)	Very limited motility in screen	Holton and Alber, 2004
	ccCor1	Homotrimeric coiled-coil domain of mammalian actin-associated protein coronin 1 (parallel, AAA-type)	Worked well in screen; Abandoned due to complications from homotrimeric form and interactions with actin	Kammerer et al., 2005
	p4	Antiparallel coiled-coil designed de novo; forms homotrimer (AAA-type)	No motility in screen	Burkhard et al., 2002
	EK Coil	Heterodimeric coiled-coil designed de novo (AB-type)	Very limited motility in screen	Litowski and Hodges, 2002

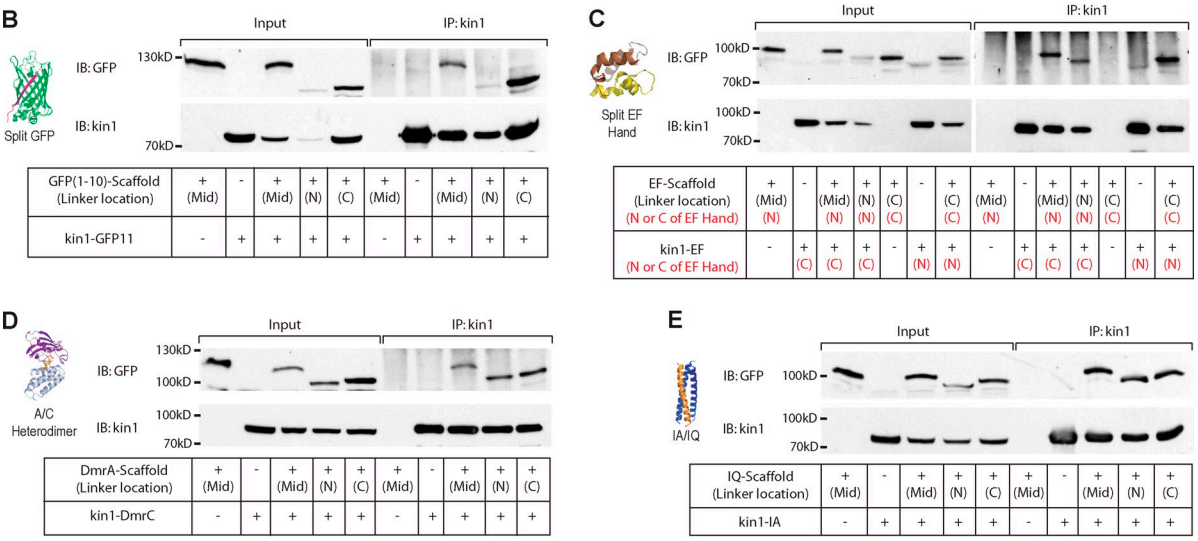

Figure S1. **Characterization of self-assembling linkers.** (A) Several potential coiled-coil linkers were screened via single molecule motility assays (see Fig. 2) to determine their suitability for assembling kin1 motors and SAH scaffolds. The heterotrimeric IA/IQ sequences were most efficient at recruiting dimeric kin1 motors to monomeric SAH scaffolds. (B–E) Coimmunoprecipitation assays. Motor–linker and linker–scaffold–GFP components were coexpressed in COS7 cells and immunoprecipitated (IP) from cell lysates with a monoclonal antibody to kin1 (IP:kin1 lanes), and the presence of scaffold was detected by immunoblotting (IB) for the GFP tag (IB:GFP). Input = 1/4 of lysate compared with IP lanes. +/− indicates the presence of the plasmid in transfection. The position of the linker with respect to the scaffold is indicated in black text as N terminus (N), middle (Mid), or C terminus (C; see Fig. 2 A). For the split GFP linker (B), the first 10 strands of the barrel (GFP(1–10)) were attached to the scaffold and the last strand (GFP11) was attached to kin1. For the split EF Hand linker (C), the red text indicates whether the N-terminal half (N) or C-terminal half (C) of the EF Hand domain was attached to the scaffold or motor components. The opposite configurations showed no assembly.

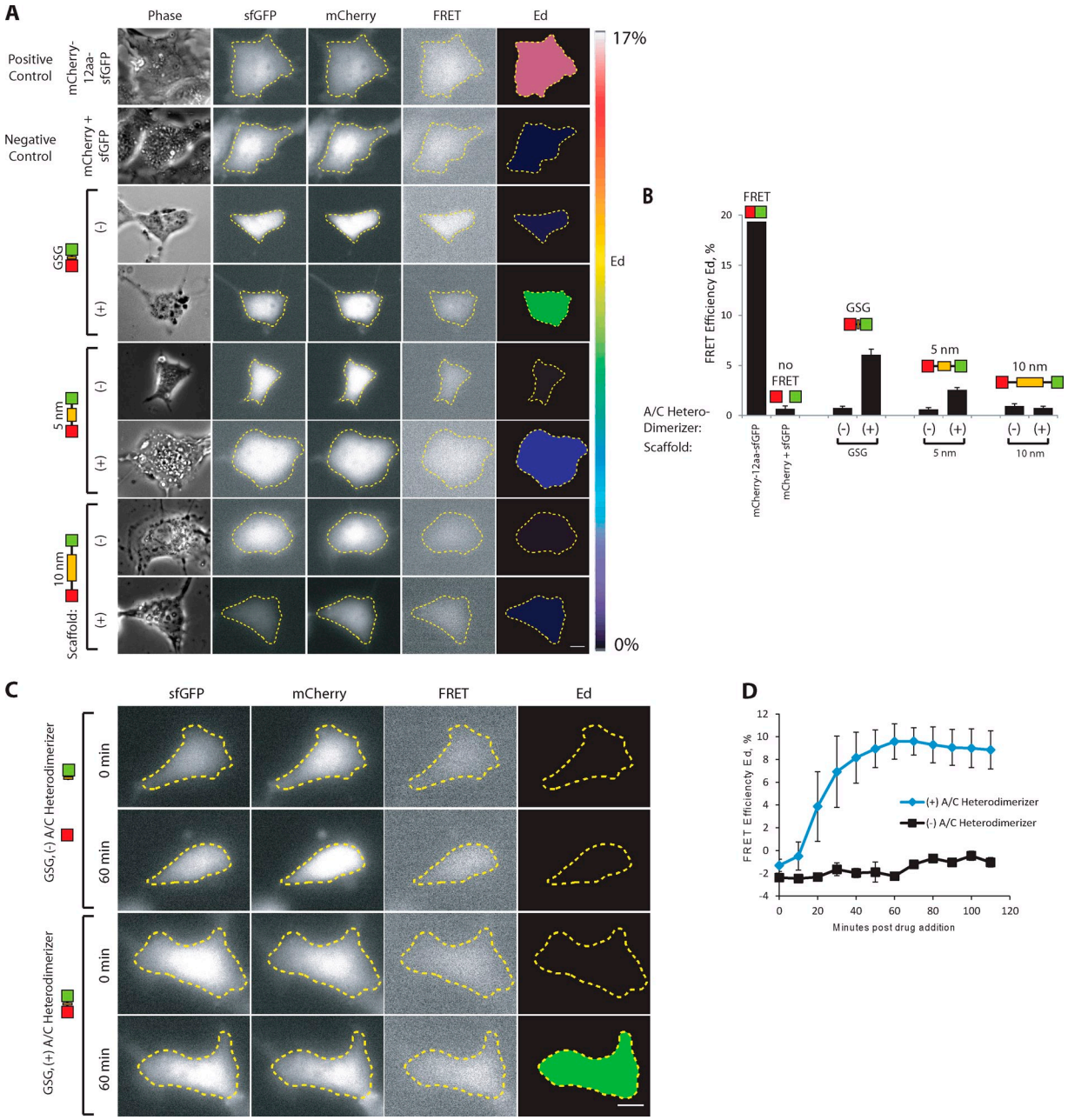

Figure S2. **Additional FRET data.** (A) Representative raw phase and fluorescence images and calculated FRET efficiency (Ed) images. For a positive FRET control, a linked mCherry-sfGFP construct was used (mCherry-12aa-sfGFP). For a negative FRET control, mCherry and sfGFP were coexpressed. All other panels indicate mCherry and split GFP separated by the indicated scaffold (GSG peptide, 5 nm SAH, or 10 nm SAH). The calculated FRET efficiency (Ed) images in rows 3–8 are shown in Fig. 3 B. Bar, 10 µm. (B) Quantification of FRET efficiency for $n = 20$ cells (controls) or ≥31 cells (scaffold) across three independent experiments. Data are presented as mean ± SD (error bars). (C and D) Time course of FRET upon addition of A/C heterodimerizer. (C) Representative raw fluorescence images and calculated FRET efficiency (Ed) images for mCherry and split GFP FRET pairs separated by a GSG peptide at 0 or 60 min after the addition of ethanol or A/C heterodimerizer. Bar, 10 µm. (D) Quantification of FRET efficiency over time. Images were acquired every 10 min and Ed was calculated from $n = 2$ (ethanol) or 3 (heterodimerizer) cells. Data are presented as mean ± SD (error bars). The broken lines indicate the outlines of each cell.

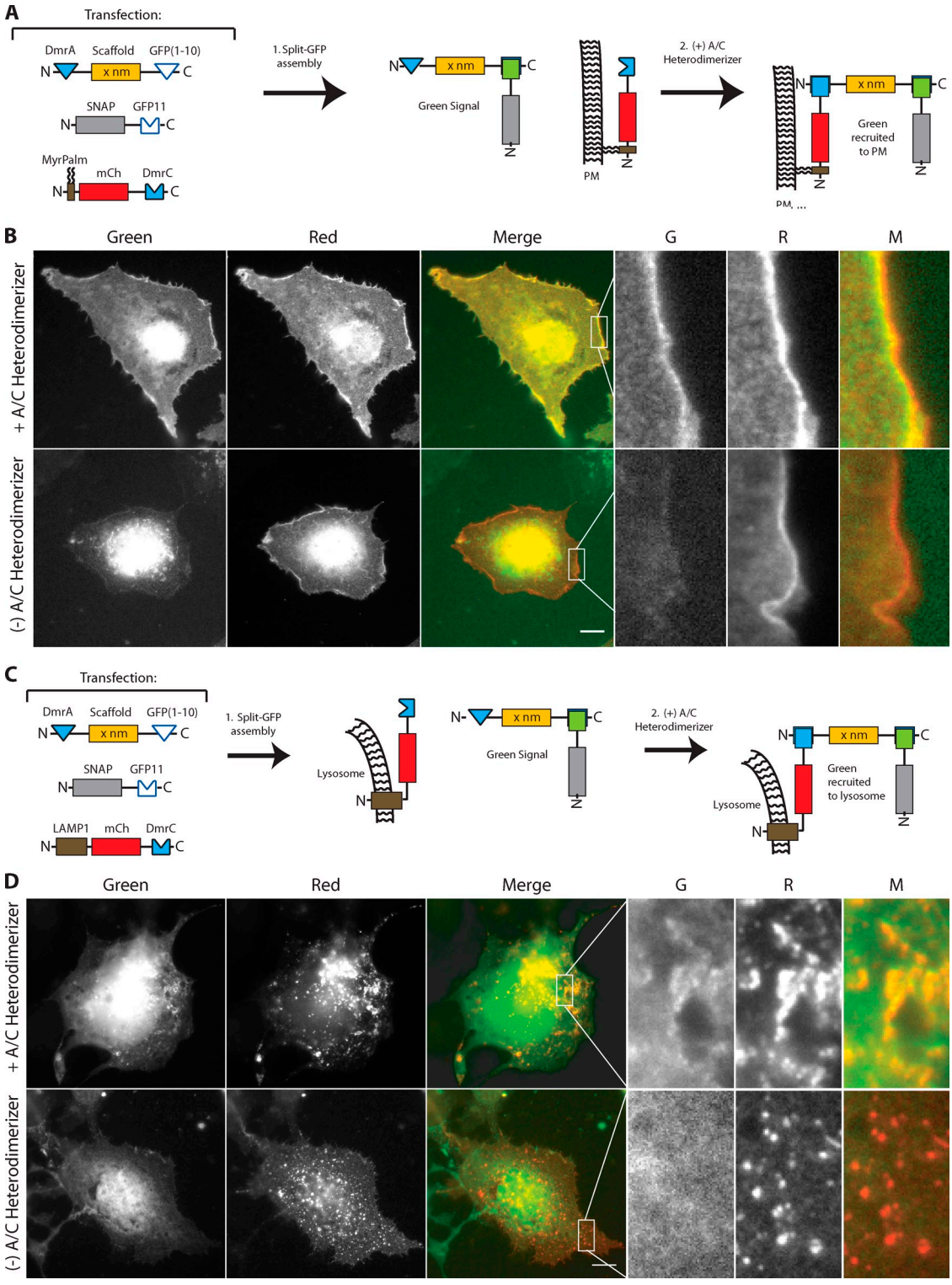

Figure S3. **Assembly of multi-protein complexes at specific subcellular locales.** (A and B) Step-wise assembly of a multi-protein complex at the plasma membrane in live cells. (A) Schematic of the experimental setup. COS7 cells were transfected with plasmids for expression of the indicated components. The split GFP self-assembles (step 1) and is recruited to the MyrPalm-mCherry component on the plasma membrane by addition of A/C heterodimerizer (step 2). (B) Representative images of cells incubated in the absence or presence of A/C heterodimerizer for 1 h. The three panels on the far right display magnified views of the boxed region in the Merge channel. Bar, 10 µm. (C and D) Step-wise assembly of a multi-protein complex on the lysosome in live cells. (C) Schematic of experimental setup. COS7 cells were transfected with plasmids for expression of the indicated components. The split GFP self-assembles (step 1) and is recruited to the LAMP1-mCherry component on the lysosome by addition of A/C heterodimerizer (step 2). (D) Images of cells incubated in the absence or presence of A/C heterodimerizer for 1 h. The three panels on the far right display magnified views of the boxed region in the Merge channel. Bar, 10 µm.

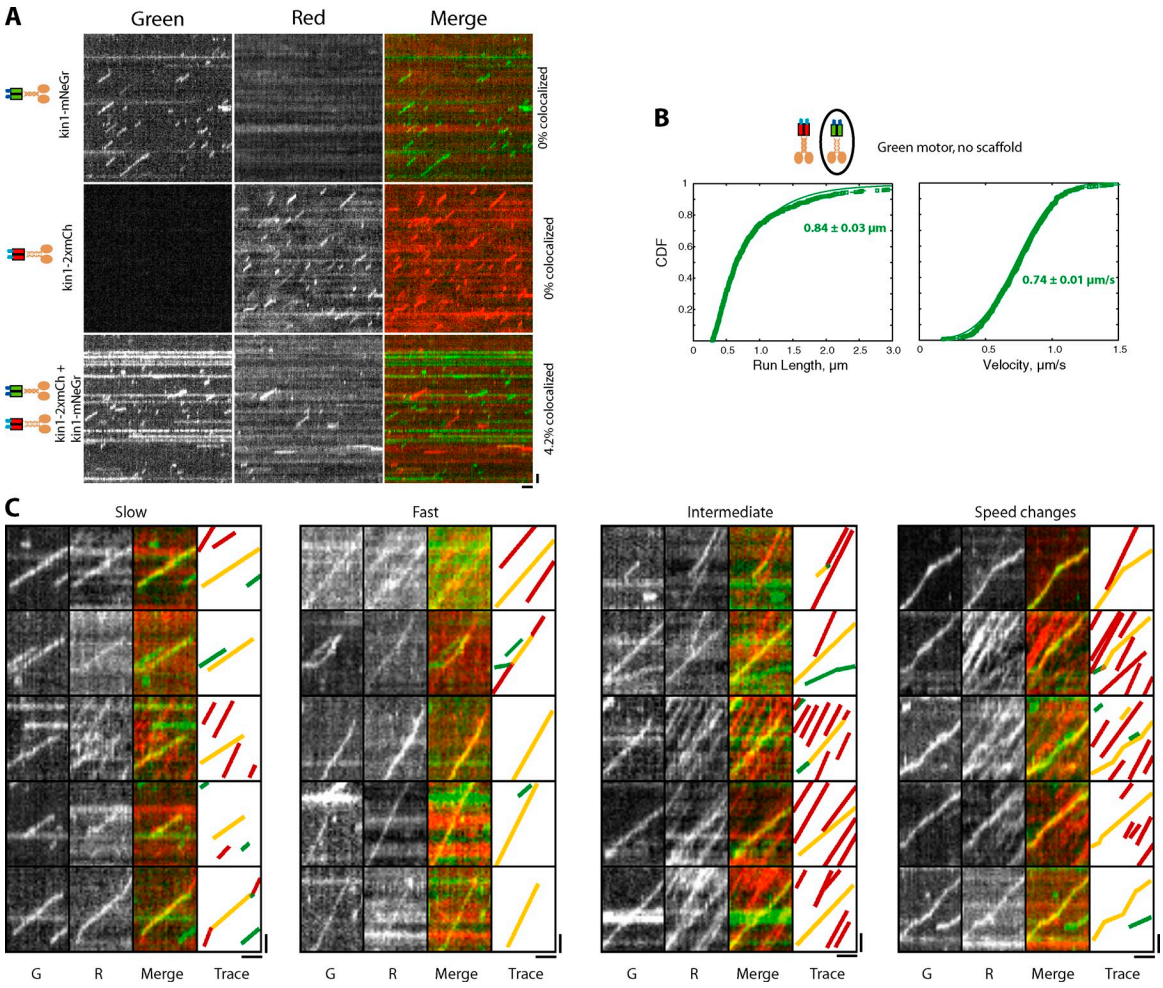

Figure S4. **Complexes of two kinesin motors analyzed in vitro.** (A and B) Motility data for single kin1 motors. (A) Representative kymographs of kin1-mNeGr expressed alone (top), kin3-2×mCh expressed alone (middle), or kin1-mNeGr and kin3-2×mCh in the absence of scaffold (bottom; shown previously in Fig. 4 B). Bars: 1 µm vertical, 1 s horizontal. The percentage colocalized indicates the percentage of two-motor events (the percentage of green events that colocalize with red events via automated tracking analysis). (B) CDFs of the run length (left) and velocity (right) for the kin1-mNeGr events when kin1-mNeGr and kin3-2×mCh were expressed in the absence of scaffold. *n* = 622 events. (C) Complexes of a fast kinesin-1 motor and a slow kinesin-3 motor analyzed in vitro. Representative kymographs of the four types of behavior observed for complexes of kin1-mNeGr + kin3-2×mCh assembled on a 20-nm scaffold and analyzed in vitro. One example in each category was shown previously in Fig. 6 D. Bars: 1 µm vertical, 1 s horizontal.

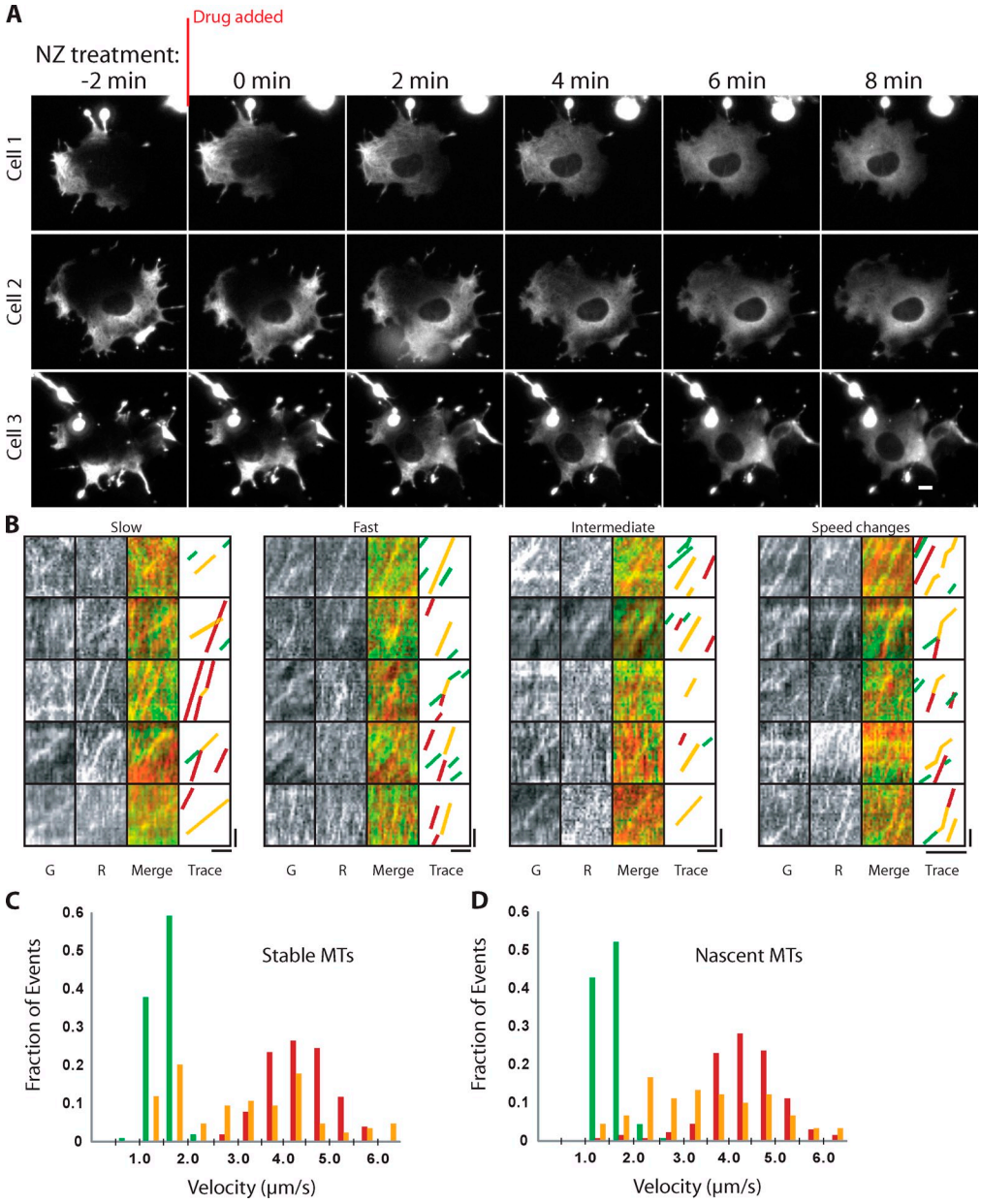

Figure S5. **NZ treatment and kin1+kin3 complexes in live COS7 cells.** (A) Live COS7 cells expressing kin3-2×mCh were imaged during NZ treatment (33 μM). Images of three representative cells before (−2 min) and after addition (0–8 min) of NZ are shown. Superprocessive kin3-2×mCh motors accumulate at the plus ends of MTs at the cell periphery but are released into the cytosol upon NZ treatment. Bar, 10 μm. (B) Representative kymographs of the four types of behavior observed for complexes of kin1-mNeGr + kin3-2×mCh assembled on a 20-nm scaffold and analyzed in live COS7 cells. One example in each category was shown previously in Fig. 7 F. Bars: 1 μm vertical, 1 s horizontal. (C and D) Velocities on stable versus nascent MTs in live COS7 cells. (C) The velocities of kin1-mNeGr (green, n = 103 events), kin3-2×mCh (red, n = 102 events), and two-motor complexes (yellow, n = 84 events) on stable MTs (NZ treatment) were determined and are plotted as a histogram for the populations. (D) The velocities of kin1-mNeGr (green, n = 138 events), kin3-2×mCh (red, n = 135 events), and two-motor complexes (yellow, n = 90 events) on nascent MTs (NZ washout) were determined and are plotted as a histogram for the populations.

Table S1. **Summary of single molecule motility events observed in this study**

Motors	Scaffold	Location	Temperature	MTs	ATP	Tracking	Velocity ± SE	Run length ± SE	*n*
							μm/s	*μm*	
kin1-mNeGr		In vitro	RT	Bovine brain	2 mM	Automated	0.74 ± 0.01	0.84 ± 0.01	622
kin1-mNeGr + kin1-2×mCh	5 nm	In vitro	RT	Bovine brain	2 mM	Automated	0.73 ± 0.01	1.07 ± 0.04	311
kin1-mNeGr + kin1-2×mCh	10 nm	In vitro	RT	Bovine brain	2 mM	Automated	0.71 ± 0.01	1.00 ± 0.03	626
kin1-mNeGr + kin1-2×mCh	20 nm	In vitro	RT	Bovine brain	2 mM	Automated	0.74 ± 0.01	1.08 ± 0.04	318
kin1-mNeGr + kin1-2×mCh	30 nm	In vitro	RT	Bovine brain	2 mM	Automated	0.64 ± 0.02	0.90 ± 0.06	124
kin1-mNeGr + kin1-2×mCh	60 nm	In vitro	RT	Bovine brain	2 mM	Automated	0.74 ± 0.01	0.95 ± 0.05	199
kin1-mNeGr		In vitro	RT	Bovine brain	20 μM	Automated	0.076 ± 0.001	1.10 ± 0.04	840
kin1-mNeGr + kin1-2×mCh	20 nm	In vitro	RT	Bovine brain	20 μM	Automated	0.081 ± 0.003	2.56 ± 0.19	116
kin1-mNeGr		In vitro	RT	Bovine brain	2 mM	Kymograph	0.80 ± 0.02	0.74 ± 0.02	207
kin3-2×mCh		In vitro	RT	Bovine brain	2 mM	Kymograph	1.76 ± 0.03	7.9 ± 0.2	211
kin1-mNeGr + kin3-2×mCh	20 nm	In vitro	RT	Bovine brain	2 mM	Kymograph	1.01 ± 0.03	3.1 ± 0.2	203
kin1-mNeGr + kin3-2×mCh "Slow"	20 nm	In vitro	RT	Bovine brain	2 mM	Kymograph	0.82 ± 0.03	2.5 ± 0.3	103
kin1-mNeGr + kin3-2×mCh "Fast"	20 nm	In vitro	RT	Bovine brain	2 mM	Kymograph	1.71 ± 0.07	3.6 ± 0.8	23
kin1-mNeGr + kin3-2×mCh "Intermediate"	20 nm	In vitro	RT	Bovine brain	2 mM	Kymograph	1.09 ± 0.03	3.0 ± 0.4	17
kin1-mNeGr + kin3-2×mCh "Speed-Change"	20 nm	In vitro	RT	Bovine brain	2 mM	Kymograph	1.02 ± 0.04	3.8 ± 0.3	60
kin1-mNeGr		COS7	37°C	All		Kymograph	1.55 ± 0.03		102
kin3-2×mCh		COS7	37°C	All		Kymograph	4.29 ± 0.05		210
kin1-mNeGr + kin3-2×mCh	20 nm	COS7	37°C	All		Kymograph	3.2 ± 0.1		106
kin1-mNeGr		COS7	37°C	Modified		Kymograph	1.55 ± 0.03		103
kin3-2×mCh		COS7	37°C	Modified		Kymograph	4.29 ± 0.07		102
kin1-mNeGr + kin3-2×mCh	20 nm	COS7	37°C	Modified		Kymograph	3.1 ± 0.2		84
kin1-mNeGr		COS7	37°C	Nascent		Kymograph	1.55 ± 0.02		138
kin3-2×mCh		COS7	37°C	Nascent		Kymograph	4.29 ± 0.07		135
kin1-mNeGr + kin3-2×mCh	20 nm	COS7	37°C	Nascent		Kymograph	3.4 ± 0.2		90

Summary of single molecule motility events observed in this study. In vitro experiments (Figs. 4–6) were performed at room temperature, whereas experiments in COS7 cells (Figs. 7 and 8) were performed at 37°C. Automated tracking was used for Figs. 4 and 5 and kymograph analysis was used for Figs. 6–8. Average velocities and run lengths are from fits to CDF, when possible. Standard error is defined as the standard deviation from bootstrapping.

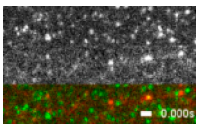

Video 1. **Motility of complexes containing two kin1 motors in vitro.** Lysates of COS7 cells expressing kin1-mNeGr-GFP11 and EF(N)-scaffold-GFP(1–10) were mixed with lysates of COS7 cells expressing kin1-2×mCh-EF(C) (see Fig. 4 A) and imaged by two-color TIRF microscopy at room temperature (Ti-E/B; Nikon). Frames were acquired continuously with 50 ms of exposure. Top, 488 nm channel; middle, 561 nm channel; bottom, merge. Particles that overlap in the 488-nm and 561-nm channels by <1 pixel are considered to be two-motor events. Bar, 1 μm.

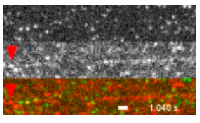

Video 2. **Motility of kin1+kin3 complexes in vitro.** Lysates of COS7 cells expressing kin1-mNeGr-GFP11, kin3-2×mCh-EF(C), and EF(N)-scaffold-GFP(1–10) (see Fig. 6 A) were imaged by two-color TIRF microscopy at RT (Ti-E/B; Nikon). Frames were acquired continuously with 50 ms of exposure. Top, 488 nm channel; middle, 561 nm channel; bottom, merge. Particles that overlap in the 488 nm and 561 nm channels by <1 pixel were considered to be two-motor events. The red arrowhead indicates a single kin3-2×mCh motor that merges with a kin1-mNeGr motor (green arrowhead) to undergo two-motor motility (yellow arrowhead) at the kin1-like speed and then splits and continues as a single kin3-2×mCh motility event (red arrowhead). Bar, 1 μm.

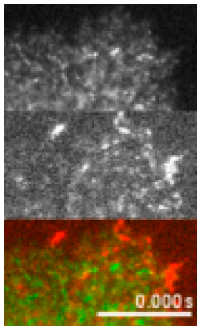

Video 3. **Motility of kin1+kin3 complexes in live cells.** COS7 cells expressing kin1-mNeGr-GFP11, kin3-2×mCh-EF(C), and EF(N)-scaffold-GFP(1–10) were briefly treated with NZ (5 min) to release motors from the MT plus ends and then imaged by two-color TIRF microscopy at 37°C (Ti-E/B; Nikon). Frames were acquired continuously with 25 ms of exposure. Top, 488 nm channel; middle, 561 nm channel; bottom, merge. Particles that overlap in the 488 nm and 561 nm channels by <1 pixel were considered to be two-motor events. Bar, 10 µm.

References

Burkhard, P., S. Ivaninskii, and A. Lustig. 2002. Improving coiled-coil stability by optimizing ionic interactions. *J. Mol. Biol.* 318:901–910. http://dx.doi.org/10.1016/S0022-2836(02)00114-6

Holton, J., and T. Alber. 2004. Automated protein crystal structure determination using ELVES. *Proc. Natl. Acad. Sci. USA*. 101:1537–1542. http://dx.doi.org/10.1073/pnas.0306241101

Kammerer, R.A., D. Kostrewa, P. Progias, S. Honnappa, D. Avila, A. Lustig, F.K. Winkler, J. Pieters, and M.O. Steinmetz. 2005. A conserved trimerization motif controls the topology of short coiled coils. *Proc. Natl. Acad. Sci. USA*. 102:13891–13896. http://dx.doi.org/10.1073/pnas.0502390102

Kiyokawa, T., K. Kanaori, K. Tajima, M. Kawaguchi, T. Mizuno, J. Oku, and T. Tanaka. 2004. Selective formation of AAB- and ABC-type heterotrimeric alpha-helical coiled coils. *Chemistry*. 10:3548–3554. http://dx.doi.org/10.1002/chem.200305729

Litowski, J.R., and R.S. Hodges. 2002. Designing heterodimeric two-stranded α-helical coiled-coils. Effects of hydrophobicity and α-helical propensity on protein folding, stability, and specificity. *J. Biol. Chem.* 277:37272–37279. http://dx.doi.org/10.1074/jbc.M204257200